Neuron
Article

Oscillatory Dynamics and Place Field Maps Reflect Hippocampal Ensemble Processing of Sequence and Place Memory under NMDA Receptor Control

Henrique O. Cabral,[1,2,3,4,*] Martin Vinck,[1,2] Celine Fouquet,[5,7,8] Cyriel M.A. Pennartz,[1,2] Laure Rondi-Reig,[5,7,8] and Francesco P. Battaglia[1,2,3,4,6,*]

[1]SILS – Center for Neuroscience, Universiteit van Amsterdam, 1090GE Amsterdam, the Netherlands
[2]Cognitive Sciences Center Amsterdam, Research Priority Program "Brain and Cognition," 1018WS Amsterdam, the Netherlands
[3]NERF, 3001 Leuven, Belgium
[4]Donders Institute for Brain Cognition and Behavior, Radboud Universiteit Nijmegen, 6500GL Nijmegen, the Netherlands
[5]Sorbonne Universités, UPMC Univ Paris 06, UMR-S 8246, Neuroscience Paris Seine, Navigation Memory and Aging Team, F-75005 Paris, France
[6]VIB, 3000 Leuven, Belgium
[7]INSERM, UMR-S 1130, Neuroscience Paris Seine, Navigation Memory and Aging Team, F-75005 Paris, France
[8]CNRS, UMR 8246, Neuroscience Paris Seine, Navigation Memory and Aging Team, F-75005 Paris, France
*Correspondence: cabralhenrique@gmail.com (H.O.C.), f.battaglia@science.ru.nl (F.P.B.)
http://dx.doi.org/10.1016/j.neuron.2013.11.010

SUMMARY

Place coding in the hippocampus requires flexible combination of sensory inputs (e.g., environmental and self-motion information) with memory of past events. We show that mouse CA1 hippocampal spatial representations may either be anchored to external landmarks (place memory) or reflect memorized sequences of cell assemblies depending on the behavioral strategy spontaneously selected. These computational modalities correspond to different CA1 dynamical states, as expressed by theta and low- and high-frequency gamma oscillations, when switching from place to sequence memory-based processing. These changes are consistent with a shift from entorhinal to CA3 input dominance on CA1. In mice with a deletion of forebrain NMDA receptors, the ability of place cells to maintain a map based on sequence memory is selectively impaired and oscillatory dynamics are correspondingly altered, suggesting that oscillations contribute to selecting behaviorally appropriate computations in the hippocampus and that NMDA receptors are crucial for this function.

INTRODUCTION

Navigation requires the coherent integration of different computations, using information about previously learned environments to respond to changing environmental demands. To navigate a previously learned route, an animal may localize itself in a pre-encoded "cognitive map," based on sensory (distal landmark) cues. For this, it may associate current position with a path to the goal (place memory in an "allocentric," world-centered reference frame). Alternatively, it may retrieve a memorized sequence of movements, independent of external information in an "egocentric," body-centered frame. In this paper, we refer to these two types of reference frames as a "place-based reference frame" and "sequence-memory-based reference frame," respectively. Allocentric (or place-learning) and simple egocentric (stimulus response-like) navigation were shown to depend, respectively, on the hippocampus (Packard and McGaugh, 1996) and dorsal striatum (Packard and McGaugh, 1996; White and McDonald, 2002). However, more recent findings implicate the hippocampus in sequential navigation when memory of multiple turns is required (Rondi-Reig et al., 2006; Iglói et al., 2010; Fouquet et al., 2010), reflecting its importance for both spatial and temporal organization of memories (Eichenbaum, 2000).

Navigational strategies based on place and sequence memory are typically jointly employed (Gothard et al., 1996b). The hippocampal subfield CA1 is at the crossroads of different information streams and may therefore be critical for combining computations underlying these strategies. Major inputs to CA1 come from CA3, crucially involved in memory retrieval (Treves and Rolls, 1994; Nakazawa et al., 2002), and from the entorhinal cortex (EC). The EC contributes to both path-integration signals (a reconstruction of current position computed from self-motion signals) from its medial subdivision (McNaughton et al., 2006; Moser and Moser, 2008) and sensory information from its lateral part (Hargreaves et al., 2005). EC inputs are critical for the emergence of CA1 place cells, neurons that fire as the animal traverses a given location (Brun et al., 2002, 2008). The precise contribution of CA3 inputs to CA1 spatial representation remains less clear (Brun et al., 2002; Nakazawa et al., 2002; Nakashiba et al., 2008), but CA1 place cells can switch between different reference frames (Jackson and Redish, 2007), possibly requiring different input streams. All of these findings suggest that inputs to CA1, most likely including CA3, can be flexibly combined to accommodate changing navigational demands.

Oscillatory coherence may help in coordinating communication across brain areas (Fries, 2005). In the hippocampal formation, gamma rhythms may modulate the interaction between

substructures (Bragin et al., 1995; Colgin et al., 2009). Low- and high-frequency gamma oscillations mediate coherence between CA1 and, respectively, CA3 and EC (Bragin et al., 1995; Colgin et al., 2009). Moreover, CA3-CA1 gamma coherence changes with cognitive demands, so that the balance between CA3 and EC inputs may be altered (Montgomery and Buzsáki, 2007). Coherence in the theta range (6–12 Hz) across hippocampal subfields can also change with behavioral state (Montgomery et al., 2009). In addition, theta organizes the fine temporal structure of hippocampal activity, enforcing a dynamical relationship between firing phase and animal position ("theta phase precession"; O'Keefe and Recce, 1993). Such fine-tuning of spike timing is thought to be crucial for synaptic plasticity (Skaggs et al., 1996).

Taken together, these data suggest that oscillatory dynamics, CA1 input selection, and the type of computation performed by the hippocampus at any given instant might be tightly related. To investigate this link, we analyzed how spatial properties and the temporal dynamics of CA1 place cells change as mice adopt different navigational strategies in a complex maze (Rondi-Reig et al., 2006). We characterized the interplay between information encoding and neural dynamics at theta (6–12 Hz), low gamma (23–40 Hz), and high gamma (55–95 Hz) frequencies, showing that different oscillatory patterns accompany different strategies.

The interplay of network connectivity and biophysical properties of neurons shapes neural oscillations. In particular, the N-methyl-D-aspartate receptor (NMDAR) is a key protein for oscillatory dynamics (Whittington et al., 1995; Middleton et al., 2008; Korotkova et al., 2010; Lazarewicz et al., 2010; Carlén et al., 2012; van Wingerden et al., 2012). In addition, it plays an important role in synaptic plasticity (Bliss and Collingridge, 1993; Tsien et al., 1996b), constructing spatial representations in CA1 (McHugh et al., 1996) and memory (Morris et al., 1986; Rondi-Reig et al., 2006). To explore NMDAR function in switching between modalities for spatial computations in the hippocampus, we used a transgenic mouse line lacking the NR1 NMDAR subunit in principal CA1 neurons (NR1-KO), with a moderate reduction of expression in deep neocortical layers (Tsien et al., 1996a; Rondi-Reig et al., 2006), whose place cells were shown to have mildly reduced spatial selectivity (McHugh et al., 1996). We found that the deficit in this transgenic mouse model concentrates on one computational modality, as place cells do not maintain a spatial map supported by sequence memory and expressed in an "egocentric" reference frame but are less affected in an "allocentric" spatial representation based on environmental cues. In control mice, these computational processes are accompanied by different regimes of oscillatory activity in the hippocampus, showing a greater involvement of theta and low gamma in sequence-based representations and high gamma for place-based representations. This variegated picture is completely disrupted in NR-1 KOs, highlighting the potential link between neural dynamics and computation.

RESULTS

Navigation Performance of Control and NR1-KO Mice

We trained control (CTR) and NR1-KO mice on a pentagon-shaped maze with five peripheral arms (the "starmaze"; Rondi-Reig et al., 2006; Figure 1A) to find food reward placed at the end of a "goal" peripheral arm. Each session contained "training trials" and "probe trials" (training trials: six or seven per pre-surgery session, 15 per recording session; probe trials: one to three per session; see Figure S1 available online for task protocol). In training trials, mice left from a fixed departure arm, but in probe trials, they started from a different peripheral arm, placed at a 72° angle with respect to the training trial departure arm (Figure 1A). Prior to surgical implant, performance of both CTR and NR1-KO mice climbed steadily (Figure 1B). However, NR1-KOs were significantly slower than CTR mice in acquiring the task (repeated-measures ANOVA: n [CTR] = 15, n [NR1-KO] = 13, $p < 0.05$). This finding confirms previous results in a water-based starmaze and a more spaced training schedule (Rondi-Reig et al., 2006). In subsequent sessions during electrophysiological recording, with different departure and goal arms and a modified cue set, learning proceeded at similar rates for the two genotypes (Figure 1B; repeated-measures ANOVA: n [CTR] = 6, n [NR1-KO] = 8, $p = 0.96$).

The starmaze task may be solved by using computations based on place or sequence memory, separately or in parallel (Rondi-Reig et al., 2006; Iglói et al., 2010). In most probe trials, control mice spontaneously followed one of two routes, allowing dissection of these strategies (Figure 1C). The first route ended in the same goal arm as in training trials, compatible with mice finding the reward on a place-based reference frame, using external landmark information. The second route reproduced the same memorized sequence of left and right turns as in training trials but from a different starting point, thereby ending in a different arm. This is compatible with subjects using a sequence-memory-based reference frame, disregarding landmark information. Probe trials were assigned to these putative reference frames based on the arm where they terminated (see Experimental Procedures). We refer to these two types of trials as "place-strategy trials" and "sequence-strategy trials." During probe trials, correct execution of either strategy resulted in reward. CTR and NR1-KO mice used both strategies in similar proportions (Figure 1D), often using both during the same recording session. In the remaining probe trials (CTR: 34%, NR1-KO: 35%), they either explored the maze by serial visits to adjacent peripheral arms or used an indistinct, random strategy.

In training and probe trials, mice traversed the maze either via a short route spanning two sides of the central pentagon or a long route spanning three sides (Figure 1A). In training trials, CTRs were as likely to use either path. NR1-KOs, however, relied mainly on the short path in training trials (Figure 1E; χ^2 test: $p < 0.001$). In place-strategy probe trials, no difference was detected between genotypes, both using predominantly the short path. During sequence-strategy trials, CTR mice used both paths in similar proportions, but NR1-KO used almost exclusively the short path (χ^2 test between genotypes: $p < 0.001$). A closer analysis shows that both genotypes made the same number of correct turns, higher than chance, at the second intersection along the long route in training trials (Figure 1F; binomial test: $p < 0.001$). However, only CTRs were above chance at the third intersection (binomial test, CTR: $p < 0.001$; χ^2 test between genotypes: $p < 0.05$). Interestingly, when examining probe trials (Figure S1), we did not find a significant difference between genotypes in

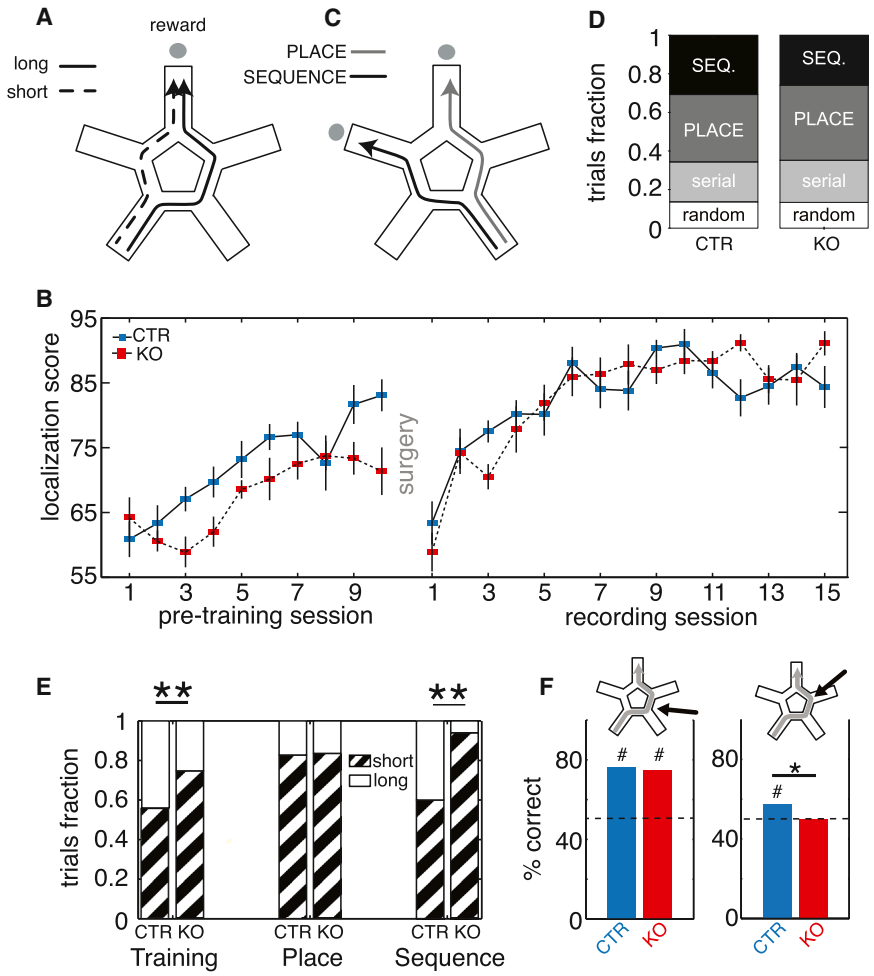

Figure 1. Learning in the Starmaze Task in Control and NR1-KO Mice

(A) Scheme of the starmaze, displaying "long" (solid line) and "short" (dashed line) paths toward the training trial reward site.

(B) "Localization score" for training trials (see Experimental Procedures), CTRs (blue), and NR1-KOs (red). Data are separated into pretraining (15 CTR and 13 NR1-KO subjects) and recording periods (6 CTR and 8 NR1-KO). In pretraining, NR1-KOs learned slower than CTRs (repeated-measures ANOVA: $p < 0.05$) but showed similar performance to CTRs during recording.

(C) Short paths used by mice during place (gray) and sequence (black) probe trials.

(D) Fraction of probe trials in which mice used, respectively, sequence strategy (SEQ.), place strategy, "serial" (defined as visiting adjacent arms sequentially), and "random" strategies during recordings. No difference was found between CTR and NR1-KO mice (Fisher's 2 × 4 exact test: p = n.s.).

(E) Percentage of short versus long trajectory to the goal, per trial type. NR1-KOs used significantly less often the long trajectory in training and sequence-strategy trials (**χ^2 test: $p < 0.001$).

(F) Percentage of correct choices at the second (left) and third (right) intersection of the long trajectory in training trials. Both genotypes performed above chance at the second intersection, but NR1-KO mice were at chance level at the third intersection. #Binomial test (versus chance): $p < 0.001$; *χ^2 test (between genotypes): $p = 0.015$. Error bars represent SEM. See also Figure S1.

the choices made at the third intersection during place-strategy trials, but we did find a strong difference during sequence-strategy trials (χ^2 test [between genotypes]: $p < 0.001$). These findings suggest that NR1-KO mice are impaired in retrieving a sequential route as a function of trajectory complexity.

There was no significant difference between genotypes or trial types in the average running speed (ANOVA: p [genotype] > 0.8, p [trial type] > 0.3, p [interaction] > 0.3; Figure S1).

Flexible Switching from Place to Sequence Reference Frame in CTR, but Not NR1-KO, Place Field Maps

From the CA1 field of the hippocampus, we recorded the activity of 952 cells from CTR mice (n = 6) and 739 cells from NR1-KO mice (n = 8). Cells were classified as either putative (inhibitory) interneurons or pyramidal cells (see Experimental Procedures and Figure S3). This sorting procedure yielded 357 and 247 pyramidal neurons with a place field from the CTR and NR1-KO groups, respectively (see Experimental Procedures). Similarly to a previous study (McHugh et al., 1996), place fields in NR1-KOs carried less spatial information than in CTRs (Figure S3).

We then examined how space-related neural activity differed between the two types of strategies spontaneously followed by mice in probe trials. In CTRs, hippocampal place fields appeared to span the same locations during place-strategy trials as in training trials (thus remaining anchored to a room-based reference frame), but in sequence-strategy trials they typically rotated together with the sequence reference frame (Figure 2 and Figure S2). To quantify these effects, we computed two similarity indices: a place-based (P_{idx}) and a sequence-based index (S_{idx}). P_{idx} was defined as the normalized Pearson's correlation between firing rate maps in training trials and place trials, using the overlapping portion of the routes (normalization was performed using a shuffling procedure; see Experimental Procedures). S_{idx} was the similarly normalized Pearson's correlation between the firing rate maps in training trials and in sequence-strategy trials, rotated by 72° to align training and probe departure arms.

CTR and NR1-KO place cells showed P_{idx} values that were several-fold higher than shuffled data, with NR1-KO showing moderately lower values than CTR (t test: $p < 0.05$; Figures 3A and S3). During sequence trials, CTR place cells displayed on average a high S_{idx}, confirming that they can maintain spatial selectivity and rotate their place fields with the departure arm (Figure 3B). Strikingly, NR1-KO place cells had a strongly reduced S_{idx} (t test: $p < 0.01$) compared to CTR, only showing remnants of a rotation effect. Importantly, in NR1-KOs, S_{idx}

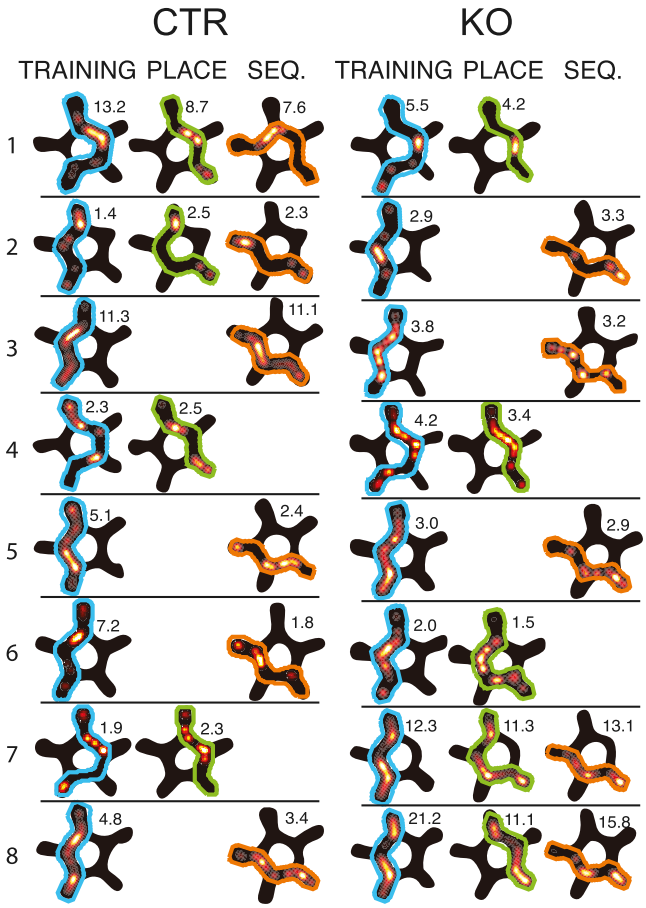

Figure 2. Place Cell Behavior during Place-Based and Sequence-Based Probe Trials

Left: example place cells in CTRs in training (mouse trajectory outlined in cyan), place-strategy (green outlines), and sequence-strategy (Seq., orange outlines) trials. The peak firing rate is indicated next to each display. Gaps correspond to sessions where that particular strategy was not expressed. Right: same as left, for NR1-KO mice.

See also Figure S2.

was significantly lower than P_{idx} (ANOVA: p [geno] < 0.01, p [trial type] < 0.01; post hoc Tukey's HSD NR1-KO: p [S_{idx} versus P_{idx}] < 0.05; see Figure S3 for details of the calculation). Moreover, in sequence trials, NR1-KO place cells showed a disrupted activity pattern, with reduced firing rates (Figure 3C; ANOVA: p [trial type] < 0.05, post hoc Tukey's HSD, NR1-KO training trial versus sequence-strategy trial: p < 0.05). Notably, in CTR mice, S_{idx} was higher when animals took the long trajectory rather than the short one (Figure 3D; t test: p < 0.01), supporting the importance of hippocampal involvement in the memory of complex movement sequences. Together, these results hint at a critical role for CA1 NMDARs in the expression of a sequence-memory-based place field map.

Differential Recruitment of Low and High Gamma Oscillations during Different Probe Trial Types

The computations involved in expressing place fields in the place or sequence reference frames may need different input streams. For example, more landmark information will be needed for processing in the place reference frame and more sequence-memory-based inputs for the sequence reference frame. Thus, the former may depend more on perforant path inputs from entorhinal cortex and the latter on Schaffer collateral inputs from CA3 (Lee and Kesner, 2003; Gilbert and Kesner, 2006). These two input structures synchronize with CA1 neural activity at different frequencies: low gamma oscillations (LG; 23–40 Hz) appear to be important for CA3-CA1 and high gamma oscillations (HG; 55–95 Hz) for EC-CA1 interactions, respectively (Colgin et al., 2009; Bragin et al., 1995). NMDARs are important for the control of gamma oscillations (Whittington et al., 1995; Middleton et al., 2008; Korotkova et al., 2010; Lazarewicz et al., 2010; Carlén et al., 2012, van Wingerden et al., 2012). This led us to explore whether there is a link between oscillatory dynamics and the observed impairment of NR1-KO place cells in switching reference.

During running periods, the CA1 pyramidal layer local field potential (LFP) was characterized by three distinct bumps in the power spectrum: theta (6–12 Hz), LG, and HG (Figures 4A and 4B). Compared to CTR, NR1-KOs showed decreased theta power and increased low frequency (<5 Hz), LG, and HG power (Figure 4B). This resembles what has been shown under pharmacological NMDAR blockade (Lazarewicz et al., 2010).

We further restricted our spectral power analysis to the different probe trial types in order to discern different power signatures underlying place and sequence navigation in CTRs and NR1-KOs. Remarkably, while no differences were found in CTRs between the two types of probe trials and training trials (Figure 4C), NR1-KOs showed increased LFP power during sequence-strategy trials in LG and HG, with respect to the already abnormally high overall values (Figure 4D). To quantify the changes across trial types, we calculated the log ratio between LG and HG power (Figure 4E). This revealed a change in the balance between LG and HG amplitude in CTRs that was dependent on the strategy being employed: while the LG and HG power ratio was similar during sequence-strategy and training trials, during place-strategy trials the ratio signaled a shift toward HG (post hoc Tukey's HSD test: p < 0.05; Kruskal-Wallis one-way ANOVA: p [trial type] < 0.05). No significant place versus sequence difference in the ratio was detected, however, in NR1-KOs. Furthermore, NR1-KOs showed a globally lower LG/HG ratio (Kruskal-Wallis one-way ANOVA: p [between genotypes] < 0.001). In summary, in CTRs, the balance between LG and HG power changed as a function of the strategy adopted during probe trials, compatible with a greater influence of CA3 inputs in sequence-strategy trials and of EC inputs in place-strategy trials. NR1-KOs, in contrast, showed relatively reduced LG power, hinting at a smaller influence of CA3 inputs.

Theta and Gamma Phase-Locking Properties of Pyramidal Cells and Interneurons in CTR and NR1-KO Mice

To study more precisely how oscillatory dynamics shape neural activity, we next analyzed the phase-locking properties of single units to different rhythms (i.e., the relative concentration of spikes at different phases) and their relationships to behavior and genotype. Trial-by-trial phase locking of single-neuron spike

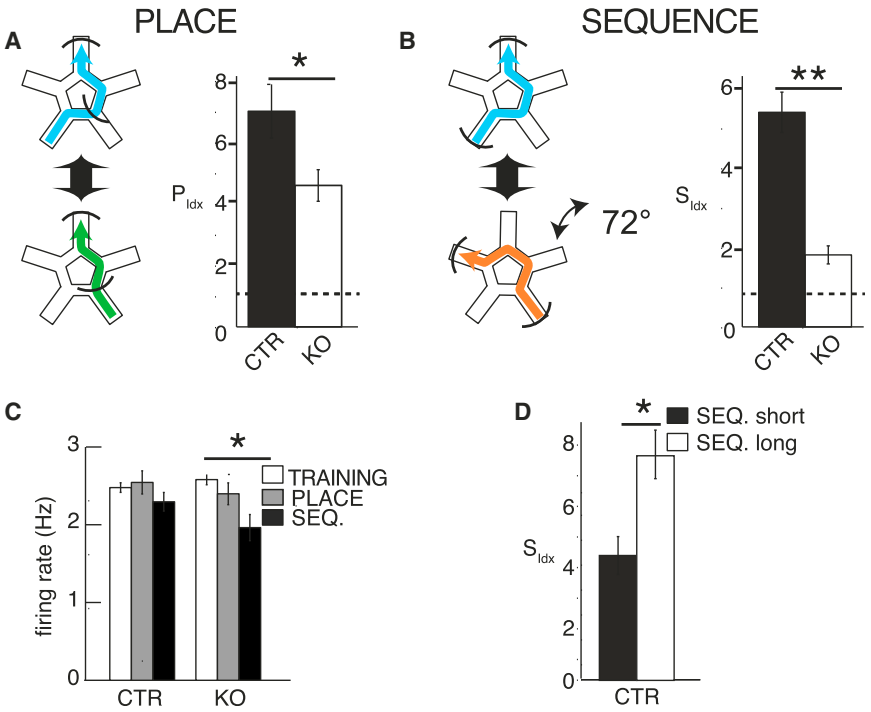

Figure 3. Impaired Expression of a Sequence Place Cell Map in NR1-KO

(A) Top: example trajectories, respectively, from training trials (cyan) and a place-strategy trial (green) used for P_{idx} (place index: similarity of firing maps between place-strategy and training trials) calculation. Parentheses indicate overlapping portions of the trajectory used for the index calculation. Bottom: average P_{idx}, for the two genotypes; NR1-KO mice showed a significantly lower value than CTRs (*t test, $p < 0.05$). Dashed line: baseline P_{idx} for shuffled data (see Experimental Procedures).

(B) Same as (A), but for S_{idx} (sequence index: similarity between the 72° rotated firing maps in sequence-strategy and the firing maps of training trials). Top: example trajectories from, respectively, training trials (cyan) and sequence-strategy trials (orange) that entered S_{idx} calculation. Before the correlation is computed, the map for the sequence-strategy trials was rotated 72° to superimpose it with the map for training trials. NR1-KOs had strongly reduced S_{idx} values with respect to CTR mice (**t test: $p < 0.01$).

(C) Average firing rate of pyramidal neurons per trial type. NR1-KO mice showed a lower firing rate during sequence-strategy trials (ANOVA: p [trial type] < 0.05; *post hoc Tukey's HSD: $p < 0.05$).

(D) Average S_{idx} for CTR mice, averaged for short and long sequence probe trials separately. S_{idx} was significantly higher for long trials (t test: $p < 0.01$). Error bars represent SEM. See also Figure S3.

trains (Figure 5) was quantified with the pairwise phase consistency (PPC) measure (Vinck et al., 2012; see Experimental Procedures). This measure of phase locking, contrary to traditional measures, remains unbiased regardless of the number of spikes in the train and is therefore applicable even to small spike samples.

The PPC spectrum computed over all trials in a session revealed that, in NR1-KOs, pyramidal neurons were on average more strongly locked than those in CTRs to the LFP in the theta and LG range ($p < 0.05$ and $p < 0.01$, respectively; Figure 5A). The fraction of significantly modulated cells was also higher in NR1-KOs for LG (Figure 5B). In the HG range, we observed a trend toward more locking in NR1-KOs, but the effect was nonsignificant, possibly due to differences in peak HG frequencies across cells. In fact, a comparison of peak values for the PPC spectrum in the HG range, as well as the LG range, for significantly locked pyramidal cells showed significantly stronger phase locking for NR1-KOs (Figure 5C; p [LG] < 0.01, p [HG] < 0.05). Similarly to pyramidal cells, NR1-KO interneurons were more phase locked to LG (Figure 5D, $p < 0.05$ and Figures 5E and 5F, $p < 0.01$), but less to theta (Figure 5D, $p < 0.05$), than CTRs. There was no difference for HG. This shows that whereas the NR1 deletion is only expressed in pyramidal cells, interneurons are affected as well, suggesting altered oscillatory modes at the network level.

Theta Phase Locking of Control Pyramidal Neurons Distinguishes between Place and Sequence Place Cells

The LFP results above suggest that oscillations in theta, LG, and HG may be associated with the computations required for maintaining place field maps in the place and sequence reference frames. To investigate this hypothesis at the single-cell level, we correlated PPC values (using spikes from all trials) with the P_{idx} (similarity index of place maps between place-strategy and training trials) and S_{idx} (similarity index of place maps between sequence-strategy and training trials) for the respective neurons. In agreement with our hypothesis, we observed a double dissociation in the theta range, with the PPC values for CTR (but not NR1-KO) neurons negatively correlated with P_{idx} but positively correlated with S_{idx}(Figures 5G and 5H; Spearman's $\rho = -0.19$, $p < 0.05$ and 0.26, $p < 0.01$, respectively; Spearman's ρ for NR1-KO: nonsignificant [n.s.]). This suggests that neurons with high theta PPC values are more likely to represent a sequence-based place cell map, whereas neurons with low theta PPC may preferentially participate in a place-based place cell representation. No significant correlations between LG and HG locking and P_{idx} or S_{idx} were observed in either genotype for pyramidal cells, possibly due to an overall low locking to these oscillations and the small spike counts, which increases the statistical variation of locking values.

The estimator variance for the unbiased PPC measure is lower for neurons with a high firing rate. Therefore, because of their higher activity, interneurons may be a more sensitive probe of the network oscillatory state on a trial-by-trial basis. We observed a strong negative correlation between LG PPC measured in sequence-strategy and place-strategy trials for CTR interneurons, suggesting that different subsets of interneurons oscillated at those frequencies during the two probe trial types (Figure 5I; CTR: Spearman's $\rho = 0.64$, $p < 0.01$). There

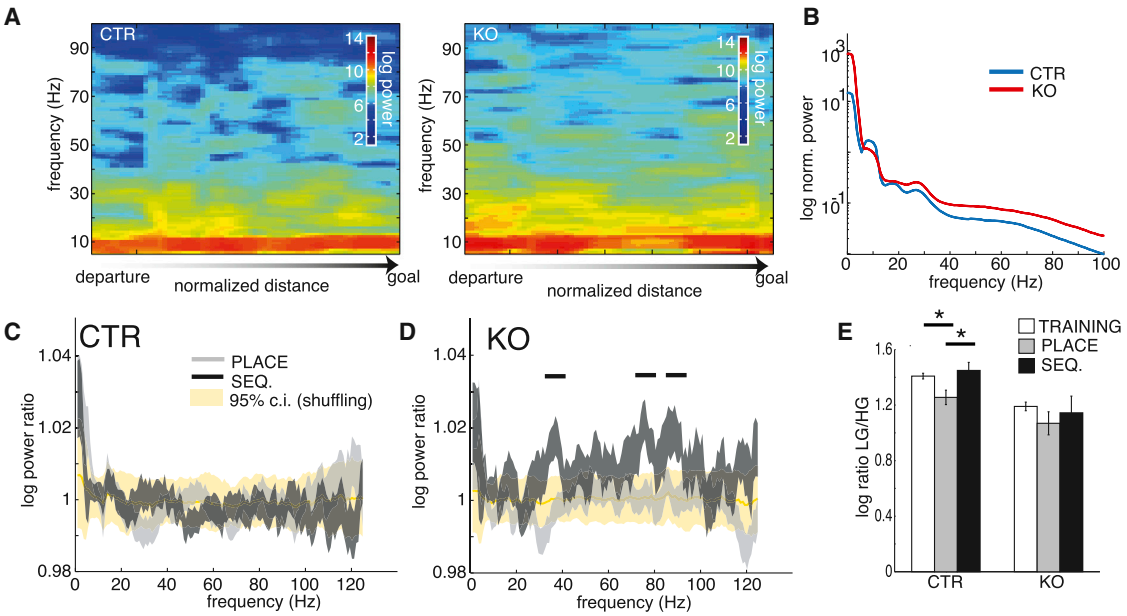

Figure 4. Increased Gamma Power in NR1-KO Mice

(A) LFP spectrograms for two example training trials from, respectively, CTRs (left) and NR1-KOs (right).

(B) Average power spectrum normalized by total power in the 4–140 Hz frequency range during all trials. NR1-KO (red) LFPs showed higher power, starting in the low gamma range (~20 Hz) and extending to all analyzed higher frequencies. Note the separation between gamma bands (LG: 23–40 Hz; HG: 55–95 Hz).

(C and D) Log power ratio in, respectively, place (light gray area: 95% confidence interval) and sequence (dark gray) trials to correct training trials (yellow area represents bootstrap 95% confidence interval computed from all trials, excluding errors). In CTRs (C), probe trial power did not differ from correct training trials. In NR1-KOs (D), power in sequence-strategy trials was significantly higher in LG and HG. Black bars: frequency range with a significant ($p < 0.05$) difference between probe trial types.

(E) Log ratio of LG to HG gamma power in training and probe trials. CTRs showed a lower LG to HG ratio in place-strategy trials compared to training and sequence-strategy trials (Kruskal-Wallis one-way ANOVA: p [trial type] < 0.05, post hoc Tukey's test: $p < 0.05$). NR1-KO did not show this effect but had an overall lower ratio (Kruskal-Wallis one-way ANOVA: p [between genotypes] < 0.001).

Error bars represent SEM.

was no such correlation in the NR1-KO interneuron population. This may indicate that different populations of interneurons phase locked to LG when different strategies were used. We also did not find a correlation in pyramidal neurons, possibly due to the lower spike count.

Behavioral Dependency of Single-Trial Theta Phase Precession

Phase locking does not fully characterize the relationship between the firing of hippocampal place cells and the theta rhythm. A negative correlation ("phase precession"; O'Keefe and Recce, 1993) exists between animal position within the cell's place field and the instantaneous firing theta phase of a place cell. While classically this phenomenon has been analyzed by pooling together spikes from multiple passages through the place fields, analytical techniques have been recently devised to quantify theta phase precession on a trial-by-trial basis (Schmidt et al., 2009; Reifenstein et al., 2012). This allowed us to compare phase precession patterns in different trial types of our task.

Most trials showed robust theta phase precession, even when as little as four spikes (which we used as threshold for inclusion in the analysis) were fired within a cell's place field (Figures 6A and S4). Following Schmidt et al. (2009) and Reifenstein et al. (2012), precession can be described by using a linear-circular model fit, with a modified Pearson's R measure used to assess goodness of fit (see Experimental Procedures). Phase precession was present across genotypes and trial types (Figure 6B). However, CTRs displayed a larger negative slope (hence, a faster precession rate) in sequence-strategy trials compared to place-strategy trials (Figure 6C; post hoc Tukey's HSD: $p < 0.05$), while NR1-KO place cells had a similar slope in all trial types. The faster precession was balanced by a decrease in place field size (Figure 6D; CTR training trial versus sequence-strategy trial: post hoc Tukey's HSD: $p < 0.05$), such that the range of the phase precession per place field traversal was maintained in all conditions (Figure 6E). These results suggest that while complete, "unitary" (Maurer et al., 2006) place fields, corresponding to one cycle of phase precession, are expressed under all conditions, in CTRs this precession takes place at a more compressed pace during sequence trials.

Interestingly, when looking at the theta phase of phase precessing spikes, we observed that spikes emitted during place-strategy trials were advanced in relation to spikes emitted during training and sequence-strategy trials, occurring most often before the trough of the theta wave (Figure 6F, left; Watson-Williams test p [training trials/sequence versus place] < 0.001). This coincides with the phase of incoming inputs from medial entorhinal cortex (mEC) layer III principal neurons

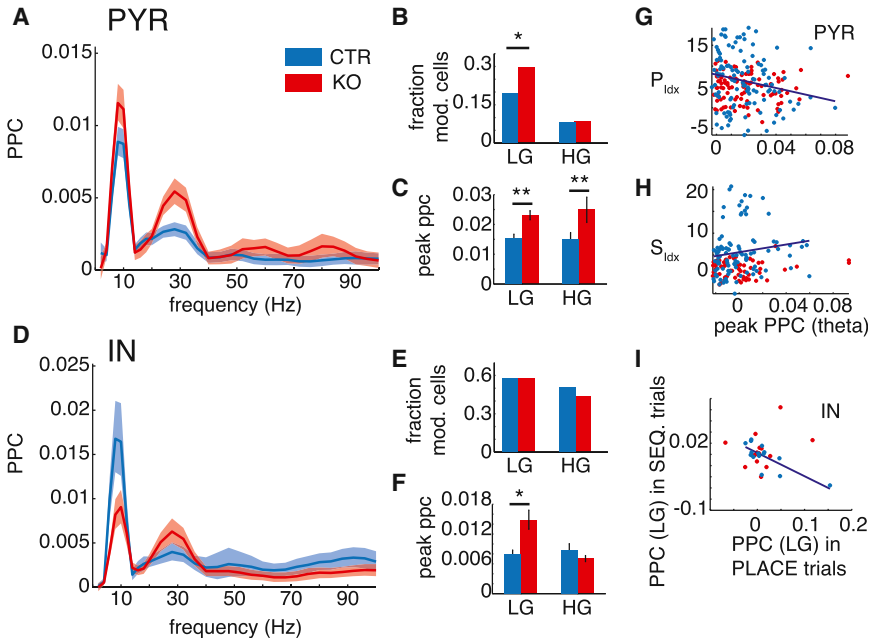

Figure 5. Pairwise Phase Consistency Spectrum for Hippocampal Neurons Modified by Probe Trial Type and Genotype

(A) Phase-locking (PPC) spectrum of pyramidal neurons of CTR and NR1-KO mice.

(B) Fraction of significantly locked pyramidal neurons to LG and HG (permutation test, corrected for multiple comparisons; *χ^2 test: $p < 0.05$).

(C) Mean of peak HG and LG PPC values for significantly locked pyramidal neurons; for each cell, the peak value of PPC within the LG and HG range, respectively, was taken. NR1-KO locking was stronger in the LG and HG range (**t test: $p < 0.01$).

(D–F) Same as (A)–(C), for interneurons.

(G and H) Scatterplot of P_{idx} (G) and S_{idx} (H) versus theta PPC (measured over all trials), for all recorded pyramidal neurons. For CTR cells, theta PPC correlated negatively with P_{idx} and positively with S_{idx}; Spearman's rho = −0.19 and 0.26, respectively; $p < 0.05$).

(I) Scatterplot of LG PPC values for interneurons in place and sequence (SEQ) trials. Values for place and sequence-strategy trials were inversely correlated (Spearman's rho = −0.64; $p < 0.05$). No correlation was observed for pyramidal cells.

Error bars represent SEM.

(Mizuseki et al., 2009; Chance, 2012). NR1-KO mice also showed this effect, though attenuated (Figure 6F, right). During sequence-strategy trials, spikes fired by NR1-KO mice occurred later than in CTRs and in training trials (WW test p [training trials versus sequence] < 0.001). These results suggest that when the place strategy is expressed, CA1 neurons are more tuned to EC inputs in control mice.

Preferred Firing Phase Shifts during Sequence Trials, Compatible with a Greater Influence of HG Modulated Inputs

The trial-type-dependent changes in the relationship between spiking activity in CA1 and theta oscillations may derive from changes in the effectiveness of EC and CA3 inputs. These two structures have different preferred spiking phases and communicate with the hippocampus via HG and LG, respectively, which occur at different theta phases (Colgin et al., 2009; Belluscio et al., 2012; Mizuseki et al., 2009) (Figures 7A, 7B, and S5). Also in our data, both CTR and NR1-KO LFPs show an earlier peak theta phase for HG than LG (Figures 7C and 7D), in relation to the peak of the theta wave. Next we calculated the cross-frequency theta modulation in each trial type (Figures 7E and 7F) and observed that, during place-strategy trials, HG-theta coherence in CTR mice was increased (Figure 7E, inset: ANOVA: p [trial type] < 0.05; post hoc Tukey's HSD p [place versus training and sequence] < 0.05). This is consistent with the results showing a higher contribution of HG oscillations during place-strategy trials (Figure 4E). NR1-KOs failed to show this effect, corroborating the results of the LG/HG power ratio of Figure 4E.

Low and High Gamma Periods Contribute Differently to Spatial Representation

Inspired by the trial-type-dependent differences observed at the LFP, spike-LFP, and LFP-LFP level, we looked at the spatial representation of single neurons during periods of predominant LG or predominant HG. For this analysis, we computed the LG-to-HG ratio per theta cycle (Figure 8A, left) and used the lower and upper quartile theta cycles as HG- and LG-dominated periods, respectively (see Experimental Procedures; Figure 8A, right). We then constructed spatial firing maps of individual cells for each probe trial, only using spikes emitted during HG and LG periods, and correlated those with the firing map calculated over all periods for the corresponding training trial (rotated by 72° for sequence-strategy trials and unrotated for place-strategy trials, similar to the overlap index calculated in Figures 3A, 3B, and 8B). This analysis revealed that, in CTR mice, the spatial firing map constructed for LG periods during sequence-strategy trials showed an increased similarity with the overall spatial firing map of corresponding training trials, in comparison with HG periods (Figure 8C; multiple t test: $p < 0.005$). This result further strengthens the link between LG oscillations and the use of sequence-memory-based navigation. NR1-KO mice did not show the same effect, in agreement with a selective disruption of CA1 patterns of activity during this type of navigation. Interestingly, despite the increased influence of HG during place navigation, as shown by a decrease in the LG/HG ratio (Figure 4E) and the higher theta-HG coherence (Figure 7E), during these probe trials, spikes emitted during LG and HG periods contributed equally to the overall spatial representation (Figure 8B).

DISCUSSION

Several studies have investigated hippocampal firing behavior when a mismatch was introduced between two reference frames, each related to a different set of sensory cues (e.g., local versus distal; Shapiro et al., 1997; Lee et al., 2004). The starmaze task allowed us to distinguish between two different strategies used by animals in route finding, one (place strategy; White

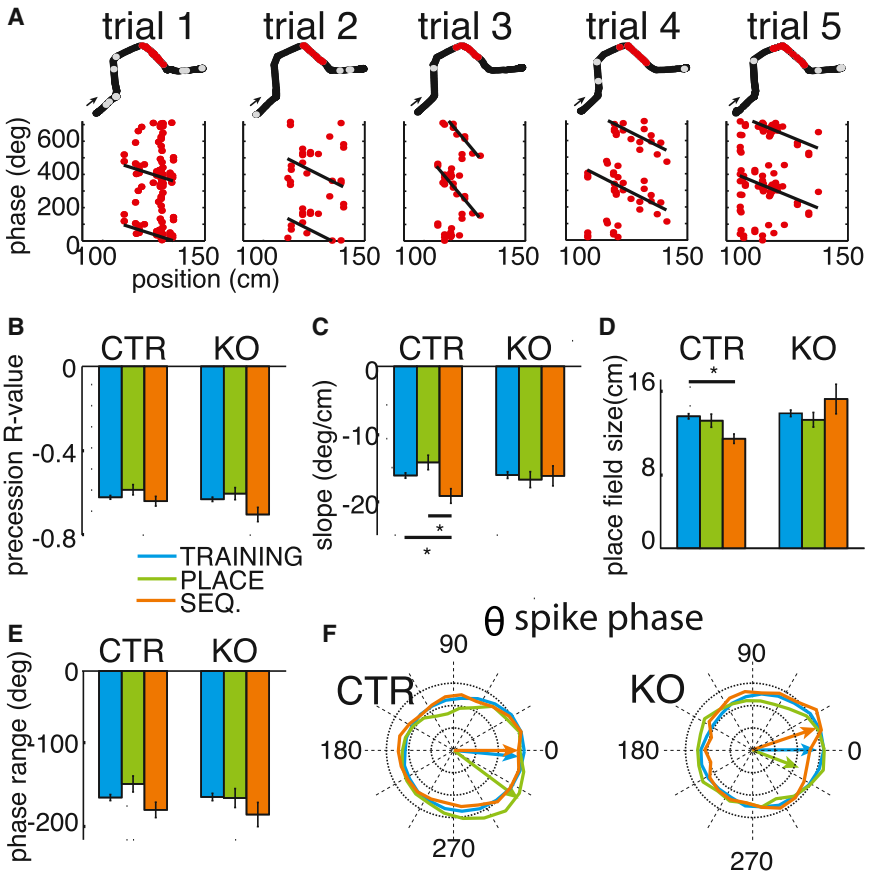

Figure 6. Single-Trial Phase Precession Analysis Highlights Faster Place Field Dynamics in Sequence-Strategy Trials in Control Mice

(A) Example of single-trial phase precession of pyramidal cells from one session (CTR mouse). Top: five trajectories for correct training trials (long path, same session). Dots represent positions at which one place cell fired during those runs. Red dots denote spikes that were fired in the cell's place field, and gray dots denote spikes fired elsewhere. Bottom: trial-by-trial position (x axis) to theta firing phase (y axis) diagram for all spikes in the place field. Theta phases are repeated over two cycles for clarity (θ,θ + 360°). The circular-linear regression line is also displayed.

(B) Average linear-circular Pearson correlation coefficient per genotype and trial type. There was an effect of trial type (two-way ANOVA: p [trial type] < 0.05), with correlation in sequence (SEQ.) trials trending to more negative values. However, this did not reach significance in post hoc tests.

(C) Average slope of the phase precession per genotype and trial type. There was a significant genotype × trial-type interaction (two-way ANOVA: p [interaction] < 0.05). Post hoc tests revealed a significant difference in sequence-strategy trials versus training and place-strategy trials in CTR pyramidal cells.

(D) Average single-trial place field size per genotype and trial type. Place fields were smaller in sequence-strategy trials in CTR mice compared to training trials (two-way ANOVA: p [interaction genotype × trial type] < 0.05). *Post hoc Tukey's test: p < 0.05).

(E) Phase range of a precession cycle per genotype and trial type. There was no significant difference between the amount of precession between genotypes and trial types.

(F) Theta phase distribution of spikes included in the phase precession analysis, per trial type, in CTR (left) and NR1-KO (right) mice. There was a significant trial type effect in both genotypes (circular ANOVA: p [trial type] < 0.01). In CTRs, this difference was due to place-strategy trials, where the spike phases were more concentrated around the descending phase of theta. Training trials and sequence-strategy trials showed a preferred phase lagging that of place-strategy trials (Watson-Williams test: p [training trials/sequence versus place] < 0.01). NR1-KO mice showed a similar pattern in place-strategy trials, but spike phases in sequence were more shifted to the early ascending theta cycle (WW-test: p [sequence versus training trials] < 0.01).

Error bars represent SEM. See also Figure S4.

and McDonald, 2002) and the other (sequence strategy) involving retrieval of a memorized sequence of body turns, disregarding all environmental cues. These strategies were spontaneously expressed in probe trials, when a rotated departure point resulted in expression of place strategy or sequence strategy in different trials. We found that the place field map and the dynamical state of the CA1 neural network changed based on the strategy spontaneously selected by the mouse, in a way that was differentially affected by NMDAR knockout. A mismatch between sensory cues and an endogenous spatial representation was also introduced by Gothard et al. (1996b) (with translated, rather than rotated, reference frames). In that study, path integration was assumed to be the source of internal information and the shift between frames occurred within each trial. In our data, the shift was correlated to the animal's self-selected behavioral strategy and the representation stayed in the same frame for the entire trial. We therefore assume that the trajectory may be compactly stored in memory as a discrete sequence of turns.

While a hippocampal involvement in place strategy (Packard and McGaugh, 1996) is expected based on its role in forming cognitive maps (McNaughton et al., 2006), simple body-turn responses are commonly linked to dorsal striatal function (Packard and McGaugh, 1996). However, sequential information necessary for memorizing longer trajectories will likely require the function of the hippocampus and CA1 in particular (Lee et al., 2005; Rondi-Reig et al., 2006). Our behavioral results support this hypothesis by revealing NR1-KO deficits in spatial decision making that relies on retrieval of complex sequences from memory (here, requiring three body turns) (Figures 1F and S1). While there are signs of memory retention for the first and second turns on the more complex path during training trials, these animals perform at chance level at the third intersection (Figure 1F). This finding is accompanied by an increased S_{idx} (similarity index of place maps between sequence-strategy and training trials) of CA1 place cells during long (three turns) versus short (two turns) sequence probe trials (Figure 3D), which also suggests that the precision of the hippocampal place cell

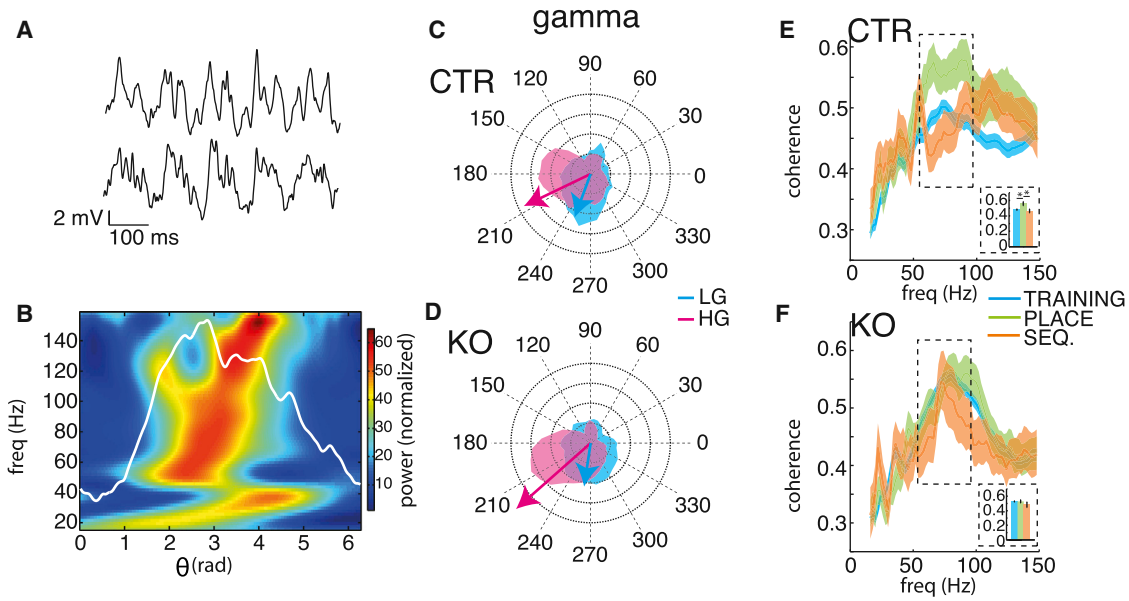

Figure 7. Intrahippocampal Cross-Frequency Synchronization and Spike-Theta Firing Suggest a Stronger Drive of CA1 Place Cells by High Gamma in Place-Strategy Trials for Control Mice

(A) Example LFP traces (CTR) highlighting co-occurrence of theta and, respectively, LG (top) and HG (bottom).

(B) Example cross-frequency comodulogram for a single trial (CTR), showing average spectral power in gamma ranges as a function of theta phase. Superimposed is the average theta cycle for the trial. Note different preferred phases for HG and LG.

(C) Polar histogram of trial-wise preferred theta phase for LG (blue shaded area) and HG (red shaded area) for all trials in CTRs. Arrows represent the mean resultant vector across all trials (in arbitrary units). There is a separation between the two distributions, with HG peaking at an earlier theta phase than LG (circular ANOVA: $p < 0.001$).

(D) Same as (C) but for NR1-KO mice; same units as in (C). Only a marginally significant difference in the mean preferred phase (circular ANOVA: $p = 0.049$) between gamma bands is found.

(E) Theta modulation of higher (>20 Hz) frequencies in CTR mice per trial type. During place-strategy trials, coherence in the HG band was augmented; inset shows average coherence in the HG band (ANOVA: p [trial type] < 0.05; post hoc: p [place versus Tr/sequence (SEQ.) trials] < 0.05).

(F) Same as (E) but for NR1-KO mice. There was no trial type effect (ANOVA: p = n.s.)

See also Figure S5.

map is related to the expression of this more complex trajectory. Hippocampal involvement is further signaled by the slower initial learning of NR1-KO mice, also shown in a water-based version of the same task (Rondi-Reig et al., 2006). The asymptotic localization score of NR1-KOs during training trials is, however, undistinguishable from that of control animals (Figure 1B), allowing fair comparison of electrophysiological correlates of maze exploration between genotypes. The unimpaired performance in the second round of training may relate to the fact that task components that are more NMDAR dependent were already acquired in pretraining and the remaining learning (e.g., new spatial layout) is relatively spared by NMDAR blockade (Bannerman et al., 1995).

Place cell dynamics in probe trials provide further hints about the possible mechanisms of hippocampal involvement in route finding: when mice spontaneously used a place strategy, place cells fired at the same location as in training trials (Figure 2). During sequence-strategy trials, CTR place cells preserved the firing sequence observed during training trials, but that sequence is expressed at spatial locations that are rotated with respect to the training trial path. Thus, the same place field map is expressed in distinct reference frames. Previous work has already shown how the place field map can dynamically change to a new configuration (Jackson and Redish, 2007) or, as it is the case here, shift to a different reference frame, translated (Gothard et al., 1996a) or rotated with respect to the original one (Gothard et al., 1996b; Kelemen and Fenton, 2010). Notably, in the present data, the reference frame shift depends on the behavior spontaneously selected by the animal, resulting in differential weight for each mechanism.

In place-strategy trials, cells are likely driven by the interplay among place memory, landmark information, and path integration (McNaughton et al., 2006). Distal visual cues are more likely to play a role in this task than local ones (Rondi-Reig et al., 2006). However, despite thorough odor neutralization following each trial, it is possible that remaining olfactory cues play a role as well.

During sequence-strategy trials, in contrast, the hippocampal representation appears less susceptible to external cues (and to disregard distal polarizing cues). Rather, one possibility is that the activity pattern observed during sequence-strategy trials may be driven by path integration (McNaughton et al., 2006). Path integration, however, is likely to play a smaller role in complex mazes, where each maze intersection acts as a path-integrator-resetting cue. This resetting behavior was indeed observed in mEC grid fields (which are hypothesized to be

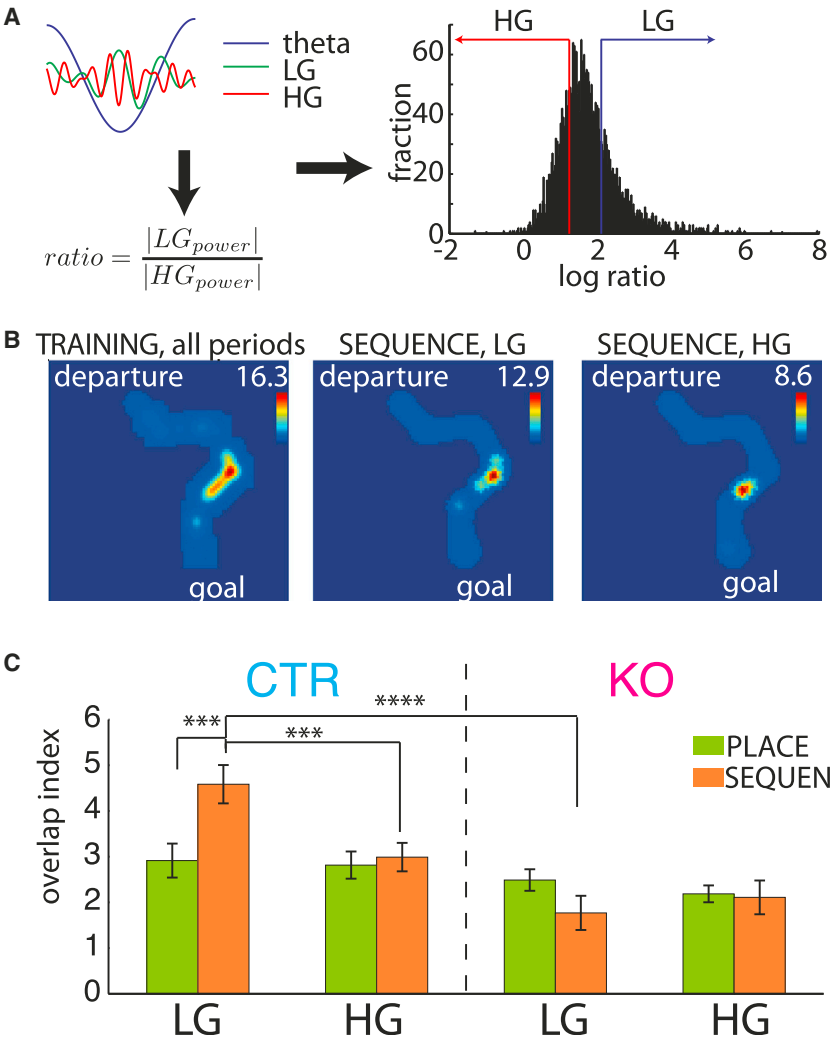

Figure 8. Low and High Gamma Carry Different Spatial Content

(A) The log ratio between low and high gamma was calculated for each theta cycle and the lower and higher quartiles were used to form spatial firing maps of LG and HG periods.

(B) Example of a CTR neuron. The firing map was calculated for all periods for each trial type (long training trial, in this case; left) and correlated with the firing map during high LG or HG periods (sequence-strategy trial in this case; middle and right, respectively); maximum firing rate is indicated in top right corner of each map.

(C) An overlap index (as in Figures 3A and 3B) for LG periods revealed that the firing map in sequence-strategy trials in CTR neurons is significantly more similar to the overall firing map in the respective training trial than that during HG periods. No effect was observed in NR1-KOs (multiple t test: ***$p < 0.005$, ****$p < 0.0001$). Error bars represent SEM.

strongly involved in path integration; Derdikman et al., 2009) as well as in CA1 place fields (Royer et al., 2010; Mizuseki et al., 2012). Another possibility is that place cell firing during sequence-strategy trials reflects the retrieval of memorized sequences of cell assemblies (Pastalkova et al., 2008; MacDonald et al., 2011), possibly stored in CA3, and paced by self-motion information or by local landmarks (e.g., maze intersections) that segment the trajectory. Interestingly, in a multi-intersection "hairpin" maze, CA1 activity was reset at each intersection, so that adjacent arms traversed sequentially were represented similarly. In contrast, CA3 activity was not (Royer et al., 2010; Mizuseki et al., 2012), suggesting that sequence information, under those conditions, is present in CA3. The CA3 input to CA1, as we will argue below, may be especially important in this situation.

Place cells in NR1-KO mice display somewhat reduced spatial information (McHugh et al., 1996). It could have been predicted that spatial representations in probe trials would also be impaired, showing a generalized degradation in all probe types. Here, however, we show that such impairment may be due to deeply and specifically disrupted activity during sequence-strategy trials, with a decreased overall firing rate and a reshuffled place field map. This suggests that whereas externally guided place memory and landmark information processing are relatively unaffected by NMDAR dysfunction in CA1, those receptors are crucial specifically for the emergence of internally driven, sequence-memory-based space representations. This sequence-based spatial representation may be especially sensitive to the disruption of synchronized firing that was shown by McHugh et al. (1996). This specific impairment may explain the moderately blurred place fields observed in this transgenic model under "normal" conditions (e.g., in training trials), when multiple sources of information are combined (McHugh et al., 1996) (Figure S3). Spatial learning deficits (Tsien et al., 1996b; Rondi-Reig et al., 2006) in NR1-KO mice could thus be interpreted as a failure to integrate memory and internal state information into a spatial map. That place field map remains, however, relatively intact and can be anchored to spatial landmarks, a function for which CA1 is ideally suited. Notably, this defective integration of information streams was measured under conditions in which task performance was unimpaired, suggesting that this particular deficit affects mostly route learning rather than the final expression of this learning.

Long-term potentiation in CA1 is impaired in NR1-KO mice (Tsien et al., 1996b), and it is plausible that memory storage and retrieval of spatial sequences are affected by reduced synaptic plasticity, e.g., in Schaffer collaterals. Conversely, transformation of EC inputs into place field-like spatial representations by the feed-forward perforant path connectivity might not need LTP/LTD (McNaughton et al., 2006; de Almeida et al., 2009). This may explain why sequence spatial maps show the most marked disruption here.

However, our neural oscillation data suggest a complementary account of the role of NMDARs. In control animals, the switch between place and sequence representations is accompanied by a reshaping of rhythms, at the population and single-cell levels, spanning theta and gamma frequencies. Such reshaping may be key to tying CA1 hippocampal responses to different input streams, giving rise to place or sequence reference frames. The dynamic reconfiguration breaks down in NR1-KO mice, which may relate to the observed lack of flexibility in spatial representations.

CA1 gamma oscillations in the LG and HG ranges have been related to, respectively, CA3 and entorhinal communication (Bragin et al., 1995; Colgin et al., 2009). In CTR mice, LG was related to memory-dominated sequence representations and HG to the place reference frame, as shown by local field potential analysis (Figure 4E). The shift in LFP power was not simply due to changes in synaptic inputs, as proposed by Bragin et al. (1995). Local neural networks were also affected, and during sequence-strategy trials, CA1 interneuron phase locking to LG predicted how well the place cell population conformed to the rotated reference frame (Figure 5I). Interestingly, the organization of HG and LG oscillations within the theta cycle was related to the expression of place fields in the appropriate reference frame for the current probe trial, as increased theta-HG coherence was observed in place-strategy trials. This raises the interesting possibility that theta-gamma interactions may be at least as important as "pure" gamma processes for ongoing computations, possibly reflecting a complex temporal coding scheme (Lisman and Jensen, 2013) and the action of O-LM interneurons, which are theta-locked and may regulate the influence of EC versus CA3 inputs (Leão et al., 2012).

Our data more directly support the link between LG, HG, and respectively sequence and place computations by showing that place field maps change depending on the currently dominating gamma frequency (Figure 8). In particular, the increased S_{idx} (similarity index between sequence and training trials) shown by CTRs during sequence-strategy trials was mainly supported by spikes emitted during dominating LG. While it is unlikely that the hippocampus ever completely "switches" from one computational mode to the other, fluctuations in oscillatory activity provided us a handle to disentangle, at least partially, the effect of different dynamic regimes directly on the place field map.

Phase-locking to theta was also related to spatial representations in different reference frames: place cells of CTR mice that were strongly theta phase locked were more likely to express a field in the sequence reference frame and less likely to express a field in the place reference frame. Single-trial phase precession also showed that, during sequence-strategy trials in CTRs, the theta phase of successive spikes changes faster as the rat traverses the place field. That is, phase precession covers similar phase ranges in all trial types, defining a complete, "unitary" place field (Maurer et al., 2006). This may be understood if in sequence-strategy trials CA1 fields are a more direct reflection of the more compact CA3 fields (Mizuseki et al., 2012).

Thus, our task allowed distinction of two different dynamical states in CA1 related, respectively, to the sequence and place reference frames. A more dominant role was played by LG and theta oscillations during sequence-strategy trials. This is compatible with a dynamics driven by retrieved sequences of cell assembly activity, originating in the CA3 recurrent network (Bragin et al., 1995; Colgin et al., 2009) and paced by theta oscillations (Pastalkova et al., 2008). During place-strategy trials, those mechanisms may to some extent subside and permit more influence from the less theta-modulated lateral entorhinal inputs (Deshmukh et al., 2010), carrying the sensory information that anchors place fields to external landmarks.

The delicate balance underlying the switch between these two dynamical states is disrupted by NMDAR dysfunction: gamma oscillations (both LG and HG) are strongly upregulated in NR1-KOs, similar to previous results from pharmacological and transgenic models (Whittington et al., 1995; Korotkova et al., 2010; Lazarewicz et al., 2010; Carlén et al., 2012). Interestingly, while previous work ascribed this effect to NMDARs on interneurons (Korotkova et al., 2010; Lazarewicz et al., 2010; Carlén et al., 2012), a similar result is reproduced here by knockout of those receptors on principal cells only. NMDARs modulate the slow components of synaptic excitatory transmission and may act as a "brake" on fast oscillations such as gamma. The effects may, therefore, reflect enhanced transmission of gamma generated in CA3 and EC (Bragin et al., 1995) in the CA1 network. The fact that interneurons are also more phase locked in NR1-KOs suggests that the CA1 network as a whole is affected by the mutation. The excess LG and HG oscillation in knockouts is most prominent during sequence-strategy trials (Figure 4D). One possibility is that, in mutants, gamma oscillations are disrupted by hypersynchrony, so that the dynamical shift to a regime supporting a memory-based reference frame cannot take place. Similarly, the reduced power of the theta signal in knockouts may contribute to the disruption of the link between theta modulation of firing and reference frames shown in Figures 5G and 5H.

In conclusion, we have shown that spontaneous strategy changes can deeply affect both the place field map and the dynamical state of CA1, possibly modifying the effective circuitry in the hippocampal formation and adjusting the performed computations so that they reflect the current behavioral demands. Changes in oscillatory regimes modulating the relative strength of different neural pathways may play a key role in these transitions, reflecting a potential general principle of brain function.

EXPERIMENTAL PROCEDURES

Subjects

Eight NR1-KO mice (Tsien et al., 1996a) and seven "floxed" littermate controls were used. All experiments were carried out in accordance with Dutch National Animal Experiments regulations (Wet op Dierproeven) and approved by the Universiteit van Amsterdam.

Behavioral Protocol

In training trials, animals had to navigate to the goal arm of the starmaze leaving from a fixed departure arm (Figure 1A). Probe trials were administered to assess the behavioral strategy used by the animals. In these trials, animals departed from a different arm. Depending on the trajectory used by the mouse, each trial was attributed to a different strategy: a probe trial resulting in a run directly to the arm rewarded in training trials was classified as a place-strategy

trial, consistent with the animal identifying the goal arm with reference to a map of the environment. If the animal used the same sequence of turns as in training trials (e.g., left-right-left turn), therefore ending in a different arm, this was interpreted as the animal executing a sequence of egocentric movements to reach the goal (sequence-strategy trial) (Figure 1C). During probe trials, both strategy choices were rewarded.

After habituation, ten sessions of pretraining were administered, including six or seven training trials and a maximum of one probe trial per session. Then, mice underwent drive implant surgery (at all times, a CTR/NR1-KO pair was studied in parallel). After recovery, 15 sessions of recording each composed of 15 training trials and two or three probe trials (from session 2) using a new configuration of departure and goal arms was chosen and a new set of environmental cues was used.

Electrophysiological Techniques

Six tetrodes (Battaglia et al., 2009) were implanted in dorsal CA1 (anteroposterior: −2.0 mm; mediolateral: −2.0 mm), guided by electrophysiological signals. Recordings were verified ex post by electrolytical lesion and Nissl stains. LFP and single-unit spikes were referred to a nearby tetrode (e.g., in corpus callosum) and digitized.

Single-unit data were presorted with KlustaKwik (Harris et al., 2000) and the result was refined using Klusters (Hazan et al., 2006). Animal position was acquired by Ethovision XT software (Noldus).

Data Analysis

Behavior

To quantify behavioral performance, we used the localization score (Fouquet et al., 2011), which was calculated by evaluating the animal's choice at each intersection; a choice bringing it closer to the goal was awarded a value of 100 (0 otherwise). The choice at the first intersection was always awarded 100. For the strategy identification in probe trials, only probe trials that were preceded by at least two equivalent correct training trials (e.g., for a short sequence probe trial, a minimum of two short training trials) since the previous probe trial were considered.

Electrophysiology

Inactivity periods (speed < 3 cm/s) were excluded from analysis.

To address the similarity of the firing rate maps between training and probe trials, we calculated two different indices. For place-strategy trials, we extracted the common occupancy area between a training trial and a place-strategy trial. For cells with at least two-thirds of its training trial place field in the common area, we calculated the P_{idx}, i.e., the Pearson's correlation between its firing map in the two conditions in that area. The S_{idx} was computed similarly, on the map rotated by 72° (Figures 3A and 3B). A normalization factor was computed by shuffling cell identities and recalculating the index.

Spectral Power Analysis

Trial-wise power spectra was determined using the Chronux toolbox (http://www.chronux.org) (bandwidth: 0–150 Hz; NW = 3; window size: 1 s).

For plots in Figures 4C and 4D, power spectra of place and sequence-strategy trials were divided by the average of the power spectra of the correct trials. Confidence intervals were obtained by 2,000-fold bootstrap.

Spike-LFP PPC Analysis

The circular concentration of spike-LFP phases was quantified using the PPC (Vinck et al., 2010; see Supplemental Experimental Procedures for mathematical formulas). LFP phase at frequency *f* was obtained by fast Fourier transforming a Hann-tapered LFP segment around each spike, with length 5/f s. Single-trial PPC was obtained using the ppc_0 quantity in Vinck et al. (2012). For multiple-trial PPC, we used ppc_1 from the same study. PPC is not biased by the number of spikes. Furthermore, ppc_1 is not affected by non-Poissonian history effects within spike trains, such as bursting, autorhythmicity, or a refractory period (Vinck et al., 2012). Its expected value equals the squared phase-locking value (i.e., the resultant length of the spike phases; Vinck et al., 2012). Significance was computed by permutation statistics (Maris et al., 2007).

Single-Trial Phase Precession Analysis

Phase precession was calculated on a trial-by-trial basis following Schmidt et al. (2009). Details are given in Supplemental Experimental Procedures.

Unless differently specified, error bars in figures represent SEM.

SUPPLEMENTAL INFORMATION

Supplemental Information includes Supplemental Experimental Procedures and five figures can be found with this article online at http://dx.doi.org/10.1016/j.neuron.2013.11.010.

AUTHOR CONTRIBUTIONS

H.O.C., L.R.-R., and F.P.B. designed the experiment. C.F. and L.R.-R. provided mice. H.O.C. performed the experiments. H.O.C., C.F., L.R.-R., and F.P.B. analyzed behavioral data. H.O.C., M.V., and F.P.B. analyzed electrophysiological data. C.M.A.P., L.R.-R., and F.P.B. supervised research. H.O.C, M.V., C.M.A.P., L.R.-R., and F.P.B. wrote the manuscript.

ACKNOWLEDGMENTS

We thank E. Holleman, T. Schröder, and Drs. C.S. Lansink, K.M. Gothard, C. Tobin, and Z. Navratilova for a critical reading of the manuscript. This work was funded by a STW grant AET7613 "MICROMAX" (to C.M.A.P.) and EU FP7 grant 270108 "Goal Leaders" (to C.M.A.P.). The project ENLIGHTENMENT 284801 (partner: F.P.B.) acknowledges the financial support of the Future and Emerging Technologies (FET) program within the Seventh Framework Program for Research of the European Commission.

Accepted: October 24, 2013
Published: January 22, 2014

REFERENCES

Bannerman, D.M., Good, M.A., Butcher, S.P., Ramsay, M., and Morris, R.G. (1995). Distinct components of spatial learning revealed by prior training and NMDA receptor blockade. Nature *378*, 182–186.

Battaglia, F.P., Kalenscher, T., Cabral, H., Winkel, J., Bos, J., Manuputy, R., van Lieshout, T., Pinkse, F., Beukers, H., and Pennartz, C. (2009). The Lantern: an ultra-light micro-drive for multi-tetrode recordings in mice and other small animals. J. Neurosci. Methods *178*, 291–300.

Belluscio, M.A., Mizuseki, K., Schmidt, R., Kempter, R., and Buzsáki, G. (2012). Cross-frequency phase-phase coupling between θ and γ oscillations in the hippocampus. J. Neurosci. *32*, 423–435.

Bliss, T.V., and Collingridge, G.L. (1993). A synaptic model of memory: long-term potentiation in the hippocampus. Nature *361*, 31–39.

Bragin, A., Jandó, G., Nádasdy, Z., Hetke, J., Wise, K., and Buzsáki, G. (1995). Gamma (40-100 Hz) oscillation in the hippocampus of the behaving rat. J. Neurosci. *15*, 47–60.

Brun, V.H., Otnass, M.K., Molden, S., Steffenach, H.A., Witter, M.P., Moser, M.B., and Moser, E.I. (2002). Place cells and place recognition maintained by direct entorhinal-hippocampal circuitry. Science *296*, 2243–2246.

Brun, V.H., Leutgeb, S., Wu, H.Q., Schwarcz, R., Witter, M.P., Moser, E.I., and Moser, M.B. (2008). Impaired spatial representation in CA1 after lesion of direct input from entorhinal cortex. Neuron *57*, 290–302.

Carlén, M., Meletis, K., Siegle, J.H., Cardin, J.A., Futai, K., Vierling-Claassen, D., Rühlmann, C., Jones, S.R., Deisseroth, K., Sheng, M., et al. (2012). A critical role for NMDA receptors in parvalbumin interneurons for gamma rhythm induction and behavior. Mol. Psychiatry *17*, 537–548.

Chance, F.S. (2012). Hippocampal phase precession from dual input components. J. Neurosci. *32*, 16693–703a.

Colgin, L.L., Denninger, T., Fyhn, M., Hafting, T., Bonnevie, T., Jensen, O., Moser, M.B., and Moser, E.I. (2009). Frequency of gamma oscillations routes flow of information in the hippocampus. Nature *462*, 353–357.

de Almeida, L., Idiart, M., and Lisman, J.E. (2009). The input-output transformation of the hippocampal granule cells: from grid cells to place fields. J. Neurosci. *29*, 7504–7512.

Derdikman, D., Whitlock, J.R., Tsao, A., Fyhn, M., Hafting, T., Moser, M.-B.B., and Moser, E.I. (2009). Fragmentation of grid cell maps in a multicompartment environment. Nat. Neurosci. *12*, 1325–1332.

Deshmukh, S.S., Yoganarasimha, D., Voicu, H., and Knierim, J.J. (2010). Theta modulation in the medial and the lateral entorhinal cortices. J. Neurophysiol. *104*, 994–1006.

Eichenbaum, H. (2000). A cortical-hippocampal system for declarative memory. Nat. Rev. Neurosci. *1*, 41–50.

Fouquet, C., Tobin, C., and Rondi-Reig, L. (2010). A new approach for modeling episodic memory from rodents to humans: the temporal order memory. Behav. Brain Res. *215*, 172–179.

Fouquet, C., Petit, G.H., Auffret, A., Gaillard, E., Rovira, C., Mariani, J., and Rondi-Reig, L. (2011). Early detection of age-related memory deficits in individual mice. Neurobiol. Aging *32*, 1881–1895.

Fries, P. (2005). A mechanism for cognitive dynamics: neuronal communication through neuronal coherence. Trends Cogn. Sci. *9*, 474–480.

Gilbert, P.E., and Kesner, R.P. (2006). The role of the dorsal CA3 hippocampal subregion in spatial working memory and pattern separation. Behav. Brain Res. *169*, 142–149.

Gothard, K.M., Skaggs, W.E., and McNaughton, B.L. (1996a). Dynamics of mismatch correction in the hippocampal ensemble code for space: interaction between path integration and environmental cues. J. Neurosci. *16*, 8027–8040.

Gothard, K.M., Skaggs, W.E., Moore, K.M., and McNaughton, B.L. (1996b). Binding of hippocampal CA1 neural activity to multiple reference frames in a landmark-based navigation task. J. Neurosci. *16*, 823–835.

Hargreaves, E.L., Rao, G., Lee, I., and Knierim, J.J. (2005). Major dissociation between medial and lateral entorhinal input to dorsal hippocampus. Science *308*, 1792–1794.

Harris, K.D., Henze, D.A., Csicsvari, J., Hirase, H., and Buzsáki, G. (2000). Accuracy of tetrode spike separation as determined by simultaneous intracellular and extracellular measurements. J. Neurophysiol. *84*, 401–414.

Hazan, L., Zugaro, M., and Buzsáki, G. (2006). Klusters, NeuroScope, NDManager: a free software suite for neurophysiological data processing and visualization. J. Neurosci. Methods *155*, 207–216.

Iglói, K., Doeller, C.F., Berthoz, A., Rondi-Reig, L., and Burgess, N. (2010). Lateralized human hippocampal activity predicts navigation based on sequence or place memory. Proc. Natl. Acad. Sci. USA *107*, 14466–14471.

Jackson, J., and Redish, A.D. (2007). Network dynamics of hippocampal cell-assemblies resemble multiple spatial maps within single tasks. Hippocampus *17*, 1209–1229.

Kelemen, E., and Fenton, A.A. (2010). Dynamic grouping of hippocampal neural activity during cognitive control of two spatial frames. PLoS Biol. *8*, e1000403.

Korotkova, T., Fuchs, E.C., Ponomarenko, A., von Engelhardt, J., and Monyer, H. (2010). NMDA receptor ablation on parvalbumin-positive interneurons impairs hippocampal synchrony, spatial representations, and working memory. Neuron *68*, 557–569.

Lazarewicz, M.T., Ehrlichman, R.S., Maxwell, C.R., Gandal, M.J., Finkel, L.H., and Siegel, S.J. (2010). Ketamine modulates theta and gamma oscillations. J. Cogn. Neurosci. *22*, 1452–1464.

Leão, R.N., Mikulovic, S., Leão, K.E., Munguba, H., Gezelius, H., Enjin, A., Patra, K., Eriksson, A., Loew, L.M., Tort, A.B., and Kullander, K. (2012). OLM interneurons differentially modulate CA3 and entorhinal inputs to hippocampal CA1 neurons. Nat. Neurosci. *15*, 1524–1530.

Lee, I., and Kesner, R.P. (2003). Time-dependent relationship between the dorsal hippocampus and the prefrontal cortex in spatial memory. J. Neurosci. *23*, 1517–1523.

Lee, I., Yoganarasimha, D., Rao, G., and Knierim, J.J. (2004). Comparison of population coherence of place cells in hippocampal subfields CA1 and CA3. Nature *430*, 456–459.

Lee, I., Jerman, T.S., and Kesner, R.P. (2005). Disruption of delayed memory for a sequence of spatial locations following CA1- or CA3-lesions of the dorsal hippocampus. Neurobiol. Learn. Mem. *84*, 138–147.

Lisman, J.E., and Jensen, O. (2013). The θ-γ neural code. Neuron *77*, 1002–1016.

MacDonald, C.J., Lepage, K.Q., Eden, U.T., and Eichenbaum, H. (2011). Hippocampal "time cells" bridge the gap in memory for discontiguous events. Neuron *71*, 737–749.

Maris, E., Schoffelen, J.M., and Fries, P. (2007). Nonparametric statistical testing of coherence differences. J. Neurosci. Methods *163*, 161–175.

Maurer, A.P., Cowen, S.L., Burke, S.N., Barnes, C.A., and McNaughton, B.L. (2006). Organization of hippocampal cell assemblies based on theta phase precession. Hippocampus *16*, 785–794.

McHugh, T.J., Blum, K.I., Tsien, J.Z., Tonegawa, S., and Wilson, M.A. (1996). Impaired hippocampal representation of space in CA1-specific NMDAR1 knockout mice. Cell *87*, 1339–1349.

McNaughton, B.L., Battaglia, F.P., Jensen, O., Moser, E.I., and Moser, M.B. (2006). Path integration and the neural basis of the 'cognitive map'. Nat. Rev. Neurosci. *7*, 663–678.

Middleton, S., Jalics, J., Kispersky, T., Lebeau, F.E., Roopun, A.K., Kopell, N.J., Whittington, M.A., and Cunningham, M.O. (2008). NMDA receptor-dependent switching between different gamma rhythm-generating microcircuits in entorhinal cortex. Proc. Natl. Acad. Sci. USA *105*, 18572–18577.

Mizuseki, K., Sirota, A., Pastalkova, E., and Buzsáki, G. (2009). Theta oscillations provide temporal windows for local circuit computation in the entorhinal-hippocampal loop. Neuron *64*, 267–280.

Mizuseki, K., Royer, S., Diba, K., and Buzsáki, G. (2012). Activity dynamics and behavioral correlates of CA3 and CA1 hippocampal pyramidal neurons. Hippocampus *22*, 1659–1680.

Montgomery, S.M., and Buzsáki, G. (2007). Gamma oscillations dynamically couple hippocampal CA3 and CA1 regions during memory task performance. Proc. Natl. Acad. Sci. USA *104*, 14495–14500.

Montgomery, S.M., Betancur, M.I., and Buzsáki, G. (2009). Behavior-dependent coordination of multiple theta dipoles in the hippocampus. J. Neurosci. *29*, 1381–1394.

Morris, R.G., Anderson, E., Lynch, G.S., and Baudry, M. (1986). Selective impairment of learning and blockade of long-term potentiation by an N-methyl-D-aspartate receptor antagonist, AP5. Nature *319*, 774–776.

Moser, E.I., and Moser, M.-B. (2008). A metric for space. Hippocampus *18*, 1142–1156.

Nakashiba, T., Young, J.Z., McHugh, T.J., Buhl, D.L., and Tonegawa, S. (2008). Transgenic inhibition of synaptic transmission reveals role of CA3 output in hippocampal learning. Science *319*, 1260–1264.

Nakazawa, K., Quirk, M.C., Chitwood, R.A., Watanabe, M., Yeckel, M.F., Sun, L.D., Kato, A., Carr, C.A., Johnston, D., Wilson, M.A., and Tonegawa, S. (2002). Requirement for hippocampal CA3 NMDA receptors in associative memory recall. Science *297*, 211–218.

O'Keefe, J., and Recce, M.L. (1993). Phase relationship between hippocampal place units and the EEG theta rhythm. Hippocampus *3*, 317–330.

Packard, M.G., and McGaugh, J.L. (1996). Inactivation of hippocampus or caudate nucleus with lidocaine differentially affects expression of place and response learning. Neurobiol. Learn. Mem. *65*, 65–72.

Pastalkova, E., Itskov, V., Amarasingham, A., and Buzsáki, G. (2008). Internally generated cell assembly sequences in the rat hippocampus. Science *321*, 1322–1327.

Reifenstein, E.T., Kempter, R., Schreiber, S., Stemmler, M.B., and Herz, A.V. (2012). Grid cells in rat entorhinal cortex encode physical space with independent firing fields and phase precession at the single-trial level. Proc. Natl. Acad. Sci. USA *109*, 6301–6306.

Rondi-Reig, L., Petit, G.H., Tobin, C., Tonegawa, S., Mariani, J., and Berthoz, A. (2006). Impaired sequential egocentric and allocentric memories in forebrain-specific-NMDA receptor knock-out mice during a new task dissociating strategies of navigation. J. Neurosci. *26*, 4071–4081.

Royer, S., Sirota, A., Patel, J., and Buzsáki, G. (2010). Distinct representations and theta dynamics in dorsal and ventral hippocampus. J. Neurosci. *30*, 1777–1787.

Schmidt, R., Diba, K., Leibold, C., Schmitz, D., Buzsáki, G., and Kempter, R. (2009). Single-trial phase precession in the hippocampus. J. Neurosci. *29*, 13232–13241.

Shapiro, M.L., Tanila, H., and Eichenbaum, H. (1997). Cues that hippocampal place cells encode: dynamic and hierarchical representation of local and distal stimuli. Hippocampus *7*, 624–642.

Skaggs, W.E., McNaughton, B.L., Wilson, M.A., and Barnes, C.A. (1996). Theta phase precession in hippocampal neuronal populations and the compression of temporal sequences. Hippocampus *6*, 149–172.

Treves, A., and Rolls, E.T. (1994). Computational analysis of the role of the hippocampus in memory. Hippocampus *4*, 374–391.

Tsien, J.Z., Chen, D.F., Gerber, D., Tom, C., Mercer, E.H., Anderson, D.J., Mayford, M., Kandel, E.R., and Tonegawa, S. (1996a). Subregion- and cell type-restricted gene knockout in mouse brain. Cell *87*, 1317–1326.

Tsien, J.Z., Huerta, P.T., and Tonegawa, S. (1996b). The essential role of hippocampal CA1 NMDA receptor-dependent synaptic plasticity in spatial memory. Cell *87*, 1327–1338.

van Wingerden, M., Vinck, M.A., Tijms, V., Ferreira, I.R., Jonker, A.J., and Pennartz, C.M.A. (2012). NMDA receptors control cue-outcome selectivity and plasticity of orbitofrontal firing patterns during associative stimulus-reward learning. Neuron *76*, 813–825.

Vinck, M., van Wingerden, M., Womelsdorf, T., Fries, P., and Pennartz, C. (2010). The pairwise phase consistency: a bias-free measure of rhythmic neural synchronization. Neuroimage *51*, 112–122.

Vinck, M., Battaglia, F.P., Womelsdorf, T., and Pennartz, C. (2012). Improved measures of phase-coupling between spikes and the Local Field Potential. J. Comput. Neurosci. *33*, 53–75.

White, N.M., and McDonald, R.J. (2002). Multiple parallel memory systems in the brain of the rat. Neurobiol. Learn. Mem. *77*, 125–184.

Whittington, M.A., Traub, R.D., and Jefferys, J.G. (1995). Synchronized oscillations in interneuron networks driven by metabotropic glutamate receptor activation. Nature *373*, 612–615.